Structured porous coated cylinder modifications based on internal flow field data

Max Scholz*
Brunel University London, Uxbridge, UB8 3PH, UK

Elias Arcondoulis†
University of Bristol, BS8 1TR, Bristol, UK

Philip Woodhead‡, Tze Pei Chong § and Edward Smith ¶
Brunel University London, Uxbridge, UB8 3PH, UK

Porous coated cylinders have been proven to reduce vortex shedding tones relative to a bare cylinder. However, many porous treatments are based on the use of very complex, open-cell structures to manipulate turbulent flow. Due to complex geometries the physical mechanisms which can be drawn are problematic to investigate due to a typically randomised porous structure. The novel 3D printed Structured Porous Coated Cylinder (SPCC), which mimics the acoustics of open-cell foam's noise closely, absolves this issue thereby allowing improved observability and modifications. This study aims to draw from previous works and to investigate modified SPCCs to further understand the internal flows which attenuate fundamental vortex shedding tones. The initial study highlighted presented a preliminary analysis on the acoustic far-field of cylindrical structures and the validation against prior works. Following on from this, this paper highlights the modifications to the existing SPCC structure to affect the regions of stagnated flow within the porous layers, to investigate how these internal flows have impacted the vortex shedding attenuating capacity of the SPCC. Conducted at Brunel University London, the acoustic data shown confirms the ability of the SPCC to significantly reduce turbulent shedding noise over its bare cylinder counterparts and the three modified SPCCs proved in importance of the streamwise communication in the internal structure of the SPCC and that the stagnation regions as stipulated by earlier studies can be filled which retains the acoustic performance and most likely reduces the drag. Lastly the removal of the ability for the flow to travel in the spanwise direction within the SPCC has shown to improve the acoustic far field radiation over the original SPCC.

I. Introduction

The application of a passive flow control to mitigate the noise produced by a stationary circular cylinder in cross-flow has become an important topic in recent years. Prominent examples include the pantographs of high-speed trains and the landing gear of aircraft [1, 2]. The acoustic radiation of a bluff body cylinder in flow comprises of a line dipole normal to the stream, associated with the lift force and another similar tone, but at double the frequency in addition to broadband noise [3–5].

In recent years, following successful attempts to tame the undesirable flow conditions by nature-inspired methods, simultaneous mitigation of the aerodynamic noise can also be realised. Owls, the pinnacle of stealth can hunt even the most adept of prey and have long attracted interests from the aeroacoustic research community. The porous structure of feathers has long been established as one of the facilitators of silent flight [6, 7]. This feature has been adapted for many engineering surfaces to combine the low-noise characteristics with human-engineering. In recent years the application of porosity to cylinders has become a fruitful endeavor and has results in reductions in both the broadband and turbulent shedding tone [1, 8, 9]. However, the issues that arise with the application of porosity and the difficulty in interpreting

*Doctoral Researcher, Department of Mechanical and Aerospace Engineering, Max.Scholz@Brunel.ac.uk, AIAA Student Member.
†Lecturer, School of Civil, Aerospace and Mechanical Engineering, Elias.Arcondoulis@bristol.ac.uk, AIAA Senior Member.
‡Research Fellow, Department of Mechanical and Aerospace Engineering, Philip.Woodhead2@brunel.ac.uk, AIAA Member.
§Reader, Department of Mechanical and Aerospace Engineering, t.p.chong@brunel.ac.uk, AIAA Member.
¶Senior Lecturer, Department of Mechanical and Aerospace Engineering, Edward.Smith@brunel.ac.uk.

the data often lay in its complexity and random structure. For the bulk of the existing literature on the application of porous materials on cylinders, some of which are highlighted above, the porous coverings are represented by a wide range of pre-made materials from acoustic foams to aluminium metal foams all of which with complex topologies. Although the open cell porous cylinder coverings demonstrate significant turbulent shedding and broadband noise attenuation benefits, the underlying internal flow fields were difficult or impossible to examine.

The studies above highlight the gap in the research which Arcondoulis et al. [10] pursued, resulting in the design and creation of the Structured Porous Coated Cylinder (SPCC). The SPCC was devised as a way to mimic the acoustic spectra of an open-cell porous cylinders with the additional benefit of its interpretability of the complex internal flow structures due to the direct line of sight through the pores in the axial and spanwise directions. The SPCC can also be simply modified owing to its simple design methodology. As highlighted in Fig. 1, the cylinder is created from a C-shaped strut which can be scaled, mirrored and rotated to make a porous ring. The ring can then be copied to create a cylindrical covering. This design also carries with it the strength that any changes to the porous topology can be altered at the source, the C-shaped strut.

Through prior research, the SPCC [10–14] has been well defined, controlled and fabricated, whilst its capability for the reduction of the bluff body vortex shedding and broadband noise is also robustly demonstrated and matched to similar open-cell porous topologies. This combination justifies supplementary research efforts to improve the understanding of the influencing parameters on the acoustic spectra, external flow mechanics and thereby form the link to further the understanding of how complex porous structures create the attenuation benefits.

This study was designed to allow for a better understanding of the influence of certain characteristics of the internal flow field of the SPCC on the development of the separated shear layer and the wake region. To this end, six cylinders were studies, two bare baseline cylinders which match the internal and external diameters of the SPCCs, the original SPCC design as seen in previous works [10–14] and three new modified versions of the SPCC were investigated in Brunel's anechoic wind tunnel. The modified SPCC's have been designed so that they influence of the spanwise and streamwise communication between the internal structure of the SPCC can be studied in addition to the third SPCC variant focusing on the influence of the stagnation regions within the cylinder. To investigate, acoustic measurements within the anechoic environment will be the first analysis tool followed by the time-averaged and unsteady velocity measurements using hot-wire anemometry within the shear layer and wake of all cylinders. The results of this works highlighted later in this paper show interesting deviations from the original SPCC and those that were modified.

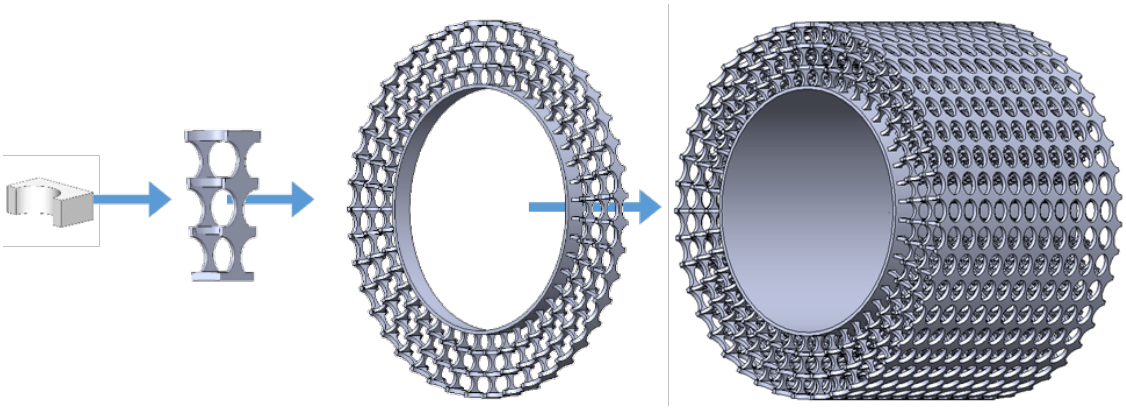

Fig. 1 CAD representation of the 3D printed SPCC and its development

II. Experimental Set-up

A. Cylinder Models

The initial study for this paper, the results of which are summarised within section. 4A, consisted of the investigation into three cylinder geometries, the SPCC which was created using an in-house Stereolithography 3D printer, and two additional extruded bare acrylic cylinders. The two acrylic cylinders act as baselines, matching both the inner diameter, signified by d, of the SPCC, shown in red in Fig. 2, and the outer diameter, signified by D, shown in highlighted blue.

The inner and outer diameters of the cylinder are 20mm and 30mm respectively. This is highlighted in Table 1 and thus the ratio of the porous coating to the to the bare cylinder diameter is 0.25. This ratio is also presented by Arcondoulis [10–14], consistent with other works [1, 15, 16]. The diameter used for the SPCC in this experiment is smaller than that previously conducted due to the smaller nozzle present at Brunel University London [17]. The blockage effect was therefore negated by reducing the outer diameter of the SPCC to mitigate any problems moving forward with this investigation.

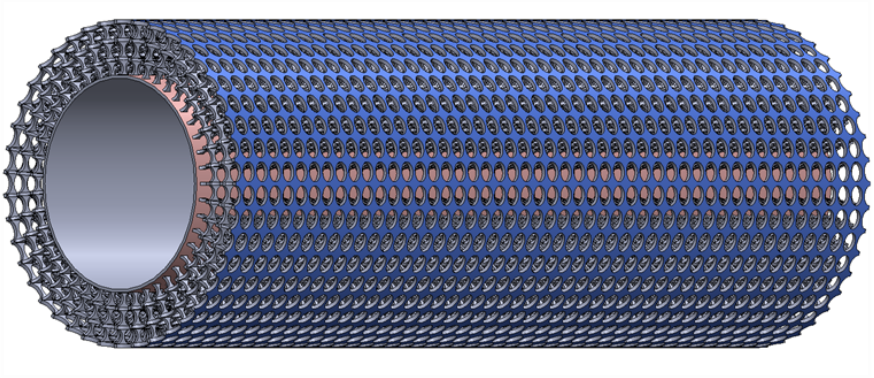

Fig. 2 CAD representation of the 3-D Printed SPCC

For reference, the porosity value of the SPCC in this investigation can be calculated using the relationship between the SPCC volume and the solid equivalent cylinder annulus:

$$\phi = 100 \cdot \frac{V_{SPCC}}{V_{CA}} \tag{1}$$

V_{SPCC} is the volume of the SPCC and V_{CA} is the solid cylinder annulus with matching inner and outer dimensions. The computer aided design software, Solidworks, was used to calculate the volume of both respective geometries and the resulting porosity value calculated was 87% porosity which directly correlate to the SPCCs used in previous studies [10, 13].

Table 1 Cylinder specifications and respective testing conditions

Type	D (mm)	U (m/s)	Re_D
SPCC	30	20 - 60	0.4 - 1.2
Bare outer cylinder	30	20 - 60	0.4 - 1.2
Bare inner cylinder	20	20 - 60	0.4 - 1.2

Based on the findings referenced above, the vortex shedding which occurs downstream of the SPCC and its variants originates from inside the porous layer, or on the inner diameter as referred to within this paper. Owing to this finding, an interesting avenue was to investigate the way in which the SPCC entrains fluid within the porous region. Whereas prior works have conducted elaborate tomographic PIV measurements, this current work will focus on the modifications

that can be made to the SPCC, based off the PIV internal flow field and the corresponding effects. One method by which the SPCC will be modified is by altering the design in a way which interferes with this communication in the spanwise direction, shown in Fig. 3c and Fig. 3b to see how the shear layers emanating from the leeward region of the cylinder effects the acoustic far-field. Another method will be to fill the stagnation regions, also highlighted in Arcondoulis et al. [13] with a solid region shown in Fig. 3a. Although undermining the main benefit of the SPCC being its non-directionality, this method might reduce the vorticity emanating from the windward side of the cylinder by increasing the velocity within the porous layer and thus altering the vortex shedding tone and frequency. All modifications to the original SPCC are presented below in Fig. 3 and their updated topologies highlighted by green regions.

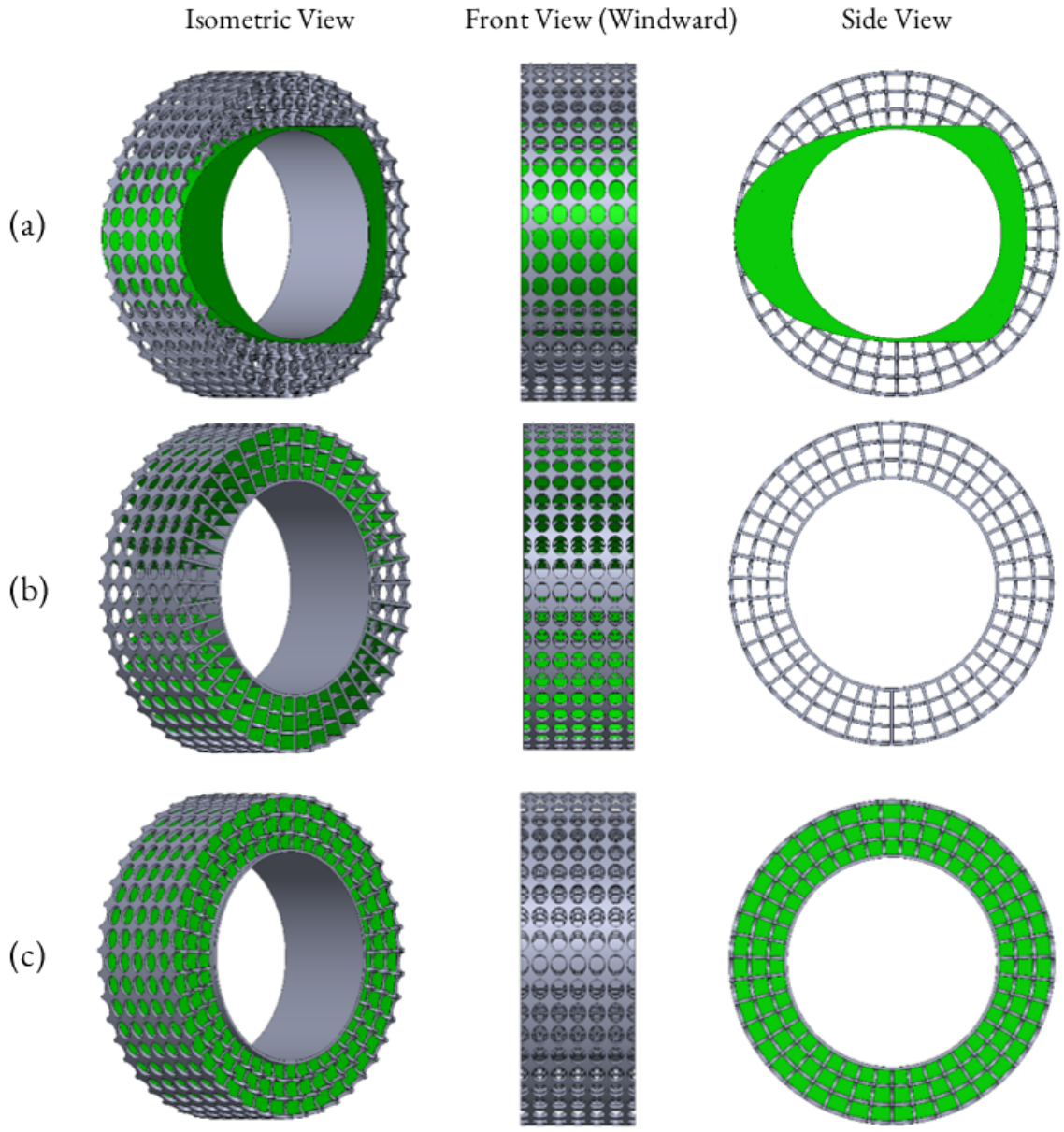

Fig. 3 CAD representations of isometric view, windward facing view and side view projections from left to right of SPCC modifications, highlighted in green are the updated geometries in relation to the base SPCC, (a) represents the Solid SPCC variant, (b) Streamwise SPCC variant and (c) Spanwise SPCC variant

B. Wind Tunnel Facilities and Instrumentation

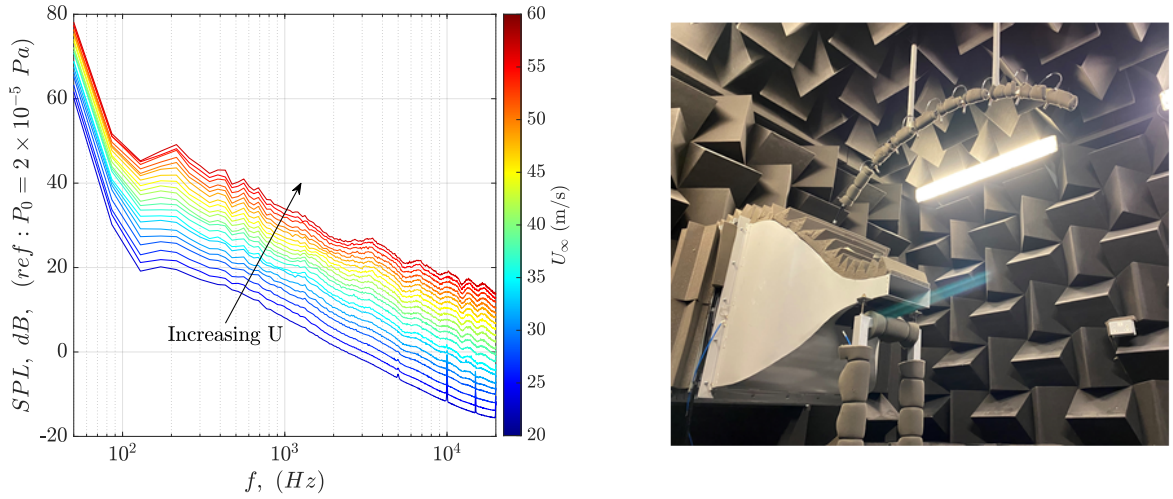

(a) **(b)**

Fig. 4 Recorded background noise measurements in Brunel's Aeroacoustic Wind Tunnel from 20 m/s to 60 m/s in increments of 2 m/s (left) and Anechoic wind tunnel facilities (right)

This section of the paper describes the anechoic wind tunnel facilities and instrumentation, shown in Fig. 4b used to measure the far-field acoustic radiations at the Brunel University London facility. As shown in Fig. 4b, the open jet wind tunnel is situated in a 4 m × 5 m × 3.4 m anechoic chamber to facilitate free field measurement of the cylinder noise. The nozzle exit is rectangular with dimensions of 0.1 m (height) × 0.3 m (width). The wind tunnel can achieve a turbulent intensity of between 0.1 - 0.2 % at a jet velocity of U_∞ = 30 m/s [17]. The maximum jet velocity can reach about 80 m/s although U_∞ values of 20 to 60 m/s in increments of 2 m/s are tested in the current study in addition to 55 m/s to align with previous studies. These correspond to Reynolds numbers based on the outer diameters of the cylinders and are listed in Table 1.

The background noise, shown in Fig. 4a, without the presence of cylinders but with the side-plates in place, is largely contributed by the low subsonic jet noise, and well below the cylinder radiated noise level produced at an identical flow speed. Situated above the cylinder are eight 0.5-inch condenser microphones (G.R.A.S 46AE) in the shape of an arc with a radius of 0.97 m. The microphones are fixed at polar angles of $50^\circ \leq \Theta \leq 120^\circ$. The polar array is positioned to coincide with the cylinder and the focal point of the arc is situated at the leeward region. A G.R.A.S 42AB sound calibrator is used to calibrate these microphones and data acquisition is facilitated by a PXIe-4464 24-bit Analogue-to-Digital card at a 44 kHz sampling frequency over a 30 second sampling time with a ± 10 dB gain automatically applied. The acquired data is then windowed and the Power Spectral Density (PSD) of 1 Hz narrow-band bandwidth is subsequently calculated using a Fast Fourier Transform with a 50% overlap. The sound pressure level (SPL) acquired by each microphone is given by

$$\mathrm{SPL} = 20 \log_{10} \left(\frac{p(f)}{p_{\mathrm{ref}}} \right), \ \mathrm{dB} \tag{2}$$

where p is the root mean square of the fluctuating acoustic pressure signal and $p_{\mathrm{ref}} = 20\ \mu$Pa is the reference pressure. The sound power level (PWL) can be calculated based on an assumption that the acoustic waves from the cylinders body are radiated in a cylindrical fashion. Firstly, the acoustic sound power, $W(f)$, is integrated for angles from Θ_1 to Θ_8 via

$$W(f) = \frac{2\pi}{\rho c_\infty} \int_{\Theta_1}^{\Theta_8} S_{pp}(f, \theta)\ \mathrm{d}\theta \tag{3}$$

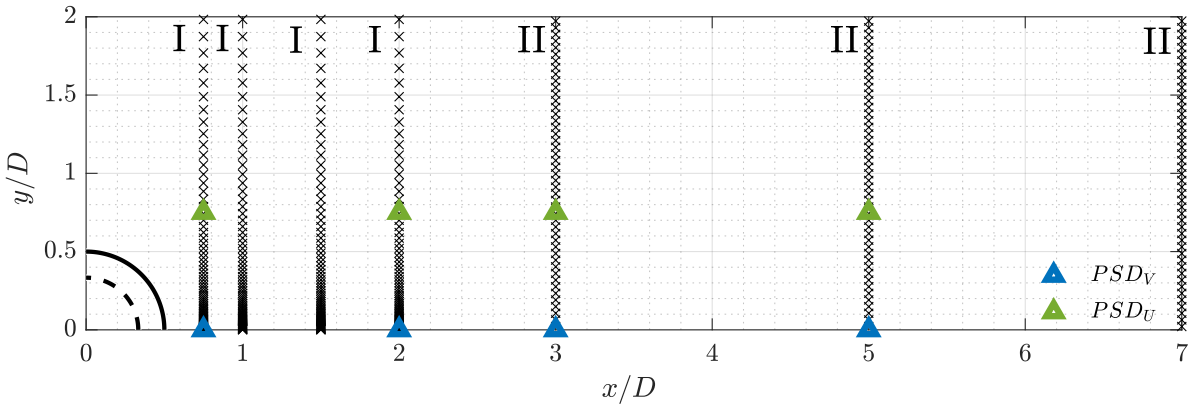

Fig. 5 A schematic diagram depicting the upper half of the map of hot-wire measurement locations used at Brunel University London, mirrored around the line y/D = 0. I stands for the 75 points in a logarithmic distribution starting with a spacing of 0.05 mm and ending with a spacing of 3.5 mm and II represents 50 points uniformly spaced with 1.25 mm spacing

where S_{pp} is the far-field pressure power spectrum density at a polar angle Θ, dΘ = 10° × $\pi/180$ represents the angle between adjacent microphones in radians, the speed of sound is c_∞ = 343 m/s and the air density is ρ = 1.225 kg/m^3.

Figure 4a displays the background noise SPL measured by the 90° polar microphone at all flow speeds considered in this study. A high frequency tonal peak is present at the lowest speeds of U_∞ = 20 to 26 m/s at 5000 Hz due to fan noise and its consequent 2nd, 3rd and 4th harmonics. This is not an issue in the spectra shown in later figures.

In the investigation into the flow field, unsteady velocity measurements were conducted at the speed of U_∞ = 40 m/s. Hotwire anemometry of the constant temperature configuration was the main diagnostic tool in the analysis of the flow field for this works. The probe used within this experiment was a DANTEC 55-P61 Cross wire probe, 5 μm in diameter and 1.25 mm in length. Interfaced by DANTEC Streamware software, the hot-wire signals were digitised by a 16-bit analogue-digital converter at a sampling frequency of 44 kHz for 10 seconds per point within the wake profile to fully quantify the properties of the oscillating structures emanating from the cylinder bodies. The hot-wire probe was mounted on a three-dimensional traverse system with a resolution of ± 0.01 mm in all directions. The probe was used to measure the mean and fluctuating velocity at several locations near the leeward region of the cylinder and into the wake. Figure 5 presents the grid and additional information regarding the distribution of points.

III. Results

A. Validation Against Prior Works

Figure 6 represents acoustic spectra measured by the 90° polar microphone. The dot-dashed red line represents the bare inner cylinder of diameter, d, and the dashed blue line represents the outer cylinder, D. As expected dominant vortex shedding tones can be seen at frequencies of ≈ 300 Hz and ≈ 490 Hz for the larger and smaller cylinder respectively with similar SPL values.

As similarly seen in previous studies on the SPCC [10–14] the SPCC exhibits similar spectral properties with a reduction of intensity of the dominant tonal peak (herein referred to as the f_1-tone) and the clearer production of a secondary tone, which will be referred to as the f_2 tone (where $f_2 = 2f_1$) in Fig. 6. The f_2 tone is discussed by Etkin et al. [3], such that the acoustic radiation from a stationary cylinder consisting of a line dipole normal to the stream, associated with the lift force and another similar tone, occurs at double the frequency. The other difference is the directionality, which is parallel to the inflow. This was further confirmed with Maryami et al. [5] and Casalino and Jacob [4] who established that the f_2 tone was due to fluctuations in drag forces acting on the cylinder in the near-wake.

Additionally, a high frequency tonal peak at a frequency of ≈ 15000 Hz is observed, although unwelcome, is expected

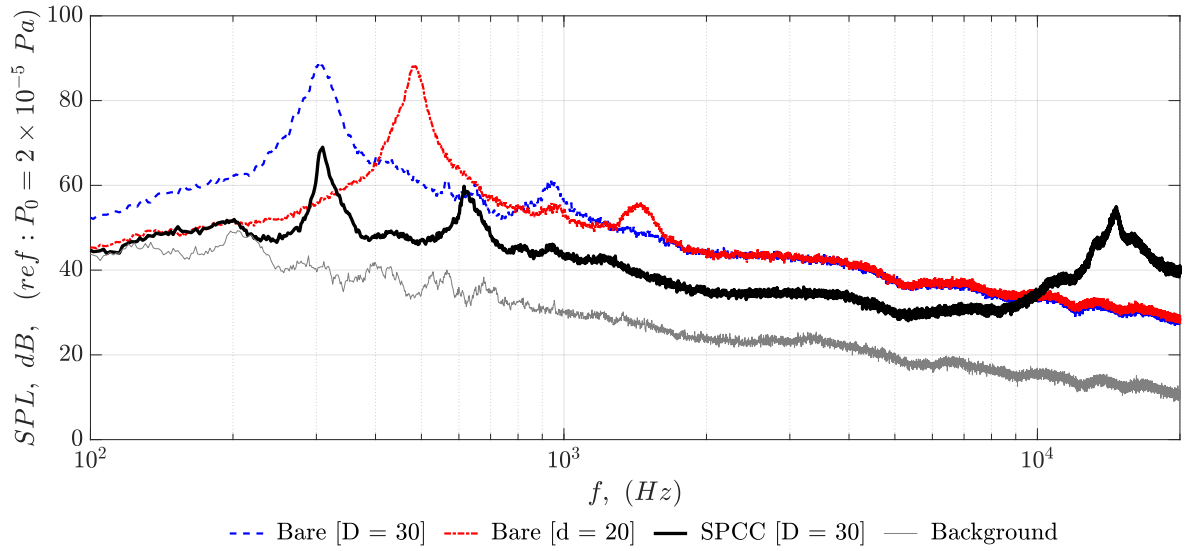

Fig. 6 SPCC and bare cylinders acoustic spectra recorded at Re_D = 1.1×10^5, Note that the Reynolds numbers correspond to the outer diameter, D, and the smaller bare cylinder, d, was subject to the same flow speeds but corresponds to a smaller Reynolds number

due to the increase in surface roughness due to the porous holes of the SPCC. This is also perceived as the underlying cause of high frequency noise in the paper by Thomas Geyer [18] in which porous aerofoils exhibited similar high frequency spectral characteristics. This same phenomenon was also found to decrease with a reduction in flow resistivity which was what suggested the surface roughness could be the cause, as the materials tested with lower flow resistivities exhibited a greater surface roughness than high flow resistivity materials. The basis of the design of the SPCC is that the acoustic spectra mimics one of an open-cell porous foam, in which case it is important to test this and ensure that the complex porosity and the SPCC match. However, at this moment in time the previous works conducted by Arcondoulis et at. [10–14] will suffice due to the similarity between the acoustic spectra recorded at Brunel University London and the Aeroacoustic Wind Tunnel in CARDC, Mianyang also very closely resembled results to a Polyurethane Porous Coated Cylinder (PUPCC) thereby confirming their similarity. In addition, the high-frequency noise generated by the SPCC is unrelated to its ability to suppress vortex shedding behaviour, which is the key aspect of its design.

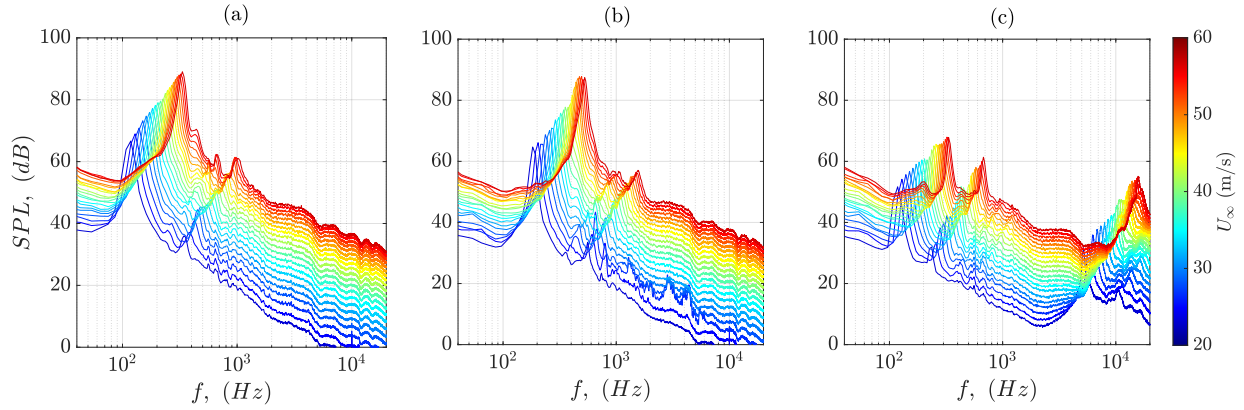

Fig. 7 SPL recorded at 90° for (a) Outer Cylinder, (b) Inner Cylinder and (c) SPCC at U_∞ = 20 m/s to 60 m/s in increments of 2 m/s

The SPL spectral plots can be seen in Fig. 7. They portray all three cylinders from 20 m/s, specified by dark blue, to 60 m/s, specified by dark red, in increments of 2 m/s. These plots clearly show the increase in the frequency of

the dominant peak throughout the Reynolds number range. This is due to the increased velocity leading to a higher frequency turbulent shedding in the wake of the cylinders. This shift in frequency can also be explained with the non-dimensional Shedding Frequency, the Strouhal number:

$$S_t = \frac{F_s \cdot d}{U_\infty} \tag{4}$$

Where F_S is the shedding frequency. Due to the small deviation of the Strouhal number based on the Reynolds number in this work [19] and the consistency of the cylinder diameter for each plot: (a), (b) and (c). The Strouhal number plots vs the SPL at the 90° polar microphone collapse as shown in Figure 8.

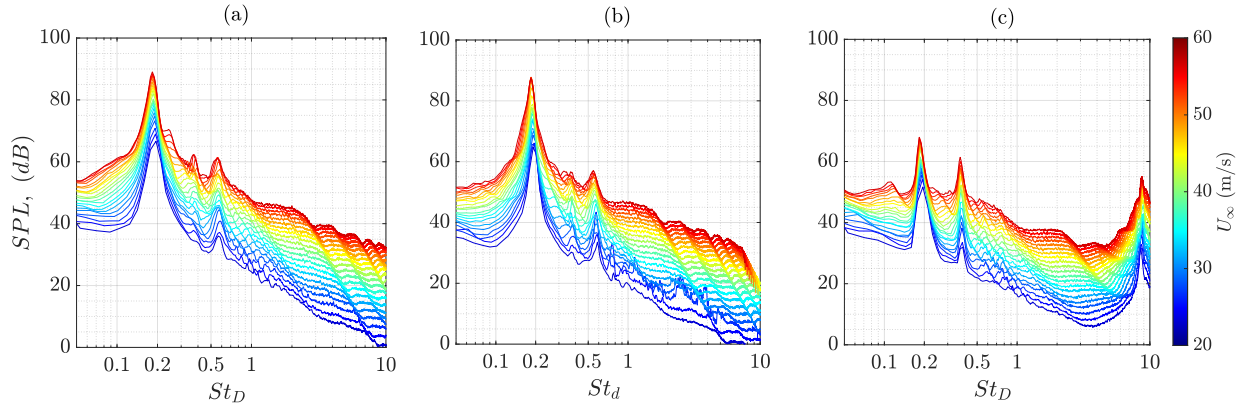

Fig. 8 SPL vs Strouhal number recorded at 90° to the flow direction for (a) Outer Cylinder, (b) Inner Cylinder and (c) SPCC at U_∞ = 20 m/s to 60 m/s in increments of 2 m/s

Figure 9 below shows this relationship between the three cylinders in clearer detail. Similarly to Fig. 6, the Reynolds number, 1.1×10^5, correspond to the outer diameter, D, of both the SPCC and larger acrylic cylinder and the smaller bare cylinder, d, was subject to the same flow speeds but corresponds to a smaller Reynolds number. The smooth bare acrylic cylinders portray the usual dominant turbulent shedding tones as expected at 88 dB and the Strouhal numbers related to the dominant tones are safely within the expected region of 0.18 – 0.19 based on the works presented by Norberg [19].

The aeroacoustics assessment performed in this initial section of the paper involves two baseline cylinders and the use of the SPCC in Brunel University London's anechoic wind tunnel. These results robustly demonstrated the capacity of the SPCC for the reduction of the vortex shedding and its consistency with previous works established in the conditions of the laboratory. Following this, further works were conducted based on these initial findings.

B. Acoustic Performance of Modified SPCCs

The SPL spectral plots for the new variations of the SPCC cylinder can be seen in Fig. 10. They portray all three cylinders from 20 m/s, specified by dark blue, to 60 m/s, specified by dark red, in increments of 2 m/s. These plots clearly show the increase in the frequency of the dominant peak throughout the Reynolds number range. This is due to the increased velocity leading to a higher frequency turbulent shedding in the wake of the cylinders. Interestingly, the deviation in their spectral characteristics is large and telling. Firstly, focusing on Fig. 10(a), which refers to the SPCC with the elimination of the spanwise communication within the internal structure, it can be seen that two peaks are still present throughout the frequency domain. However, they both show a much lower intensity. The high frequency broadband frequency range is still present and very similar to the Solid SPCC presented in subplot (c) and the original SPCC presented in Fig. 7(c).

Figure 10(b) presents to the same spectral plot for the SPCC variation with the blocked streamwise communication. As expected this has severely reduced the capability of the SPCC to reduce noise. These spectral results present similar characteristics to the baseline outer cylinder shown in Fig. 7(c). This is likely a response to the limited streamwise

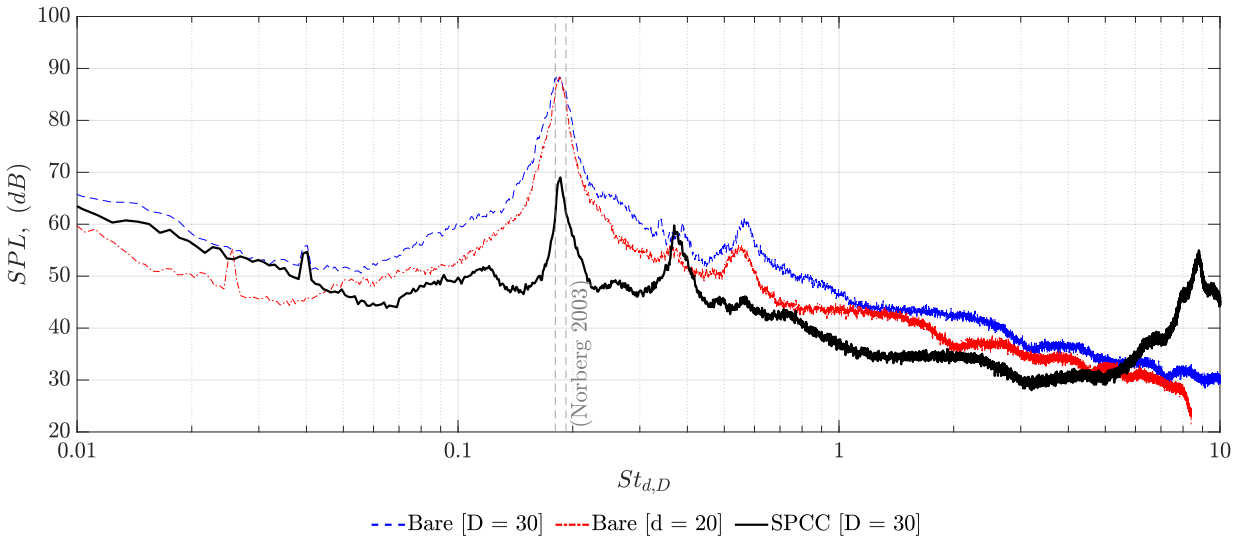

Fig. 9 Acoustic spectra vs Strouhal number of the 3D printed SPCC and both cylinder at a Re_D = 1.1×10^5. The grey vertical dashed lines refer to a published Strouhal number envelope for smooth bare cylinders [19].

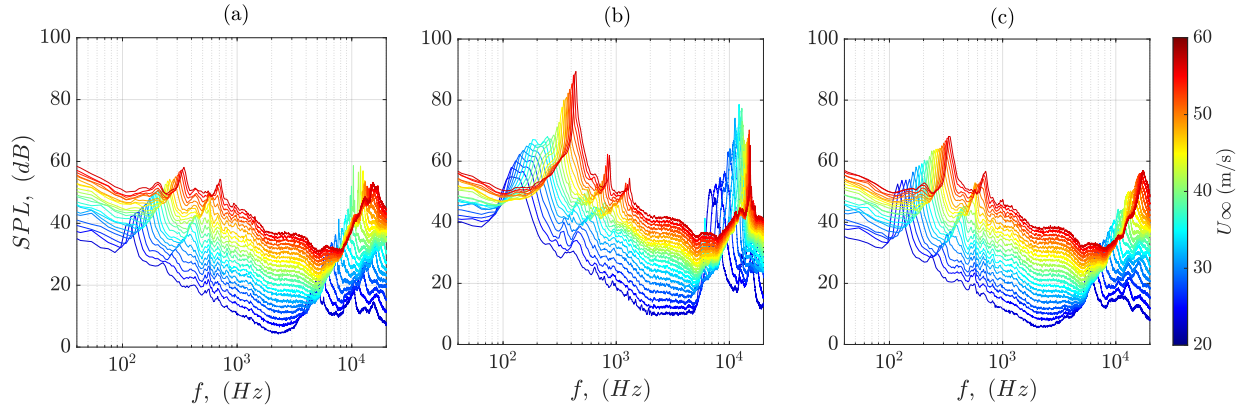

Fig. 10 SPL acoustic spectra recorded by the 90° microphone for (a) Spanwise SPCC, (b) Streamwise SPCC and (c) the Solid SPCC at U_∞ = 20 m/s to 60 m/s in increments of 2 m/s

communication reducing the performance of the SPCC similar to that of a baseline cylinder as the porous regions become stagnation regions thus acting like a larger outer cylinder.

Figure 10(c) presents the spectral plot of the SPCC variation with the solid inner aerodynamic region to mimic that of the stagnation regions of the original SPCC. Although diminishing the advantage of the SPCC with this inclusion of the aerodynamic region, reducing its directionality it should allow for further investigation into the stagnation regions and their effects. Although this SPCC variation has a large geometric deviation to the original SPCC, the spectral characteristics are extremely similar further confirming the regions of stagnation and that their removal has not changed the noise spectra significantly. This implies that the stagnation flow region first observed by Arcondoulis et al. [20] has negligible impact on the acoustic generation mechanism of an SPCC and that the SPCC naturally develops a stagnation region within its innermost porous layer on the windward side.

Figure 11 represents acoustic SPL spectra measured by the 90° polar microphone at a freestream velocity of 40 m/s. The dot-dashed blue line represents the bare outer cylinder (D = 30mm), and the orange line, the standard original SPCC with the same diameter, D. As expected dominant turbulent shedding tones can be seen at frequencies of ≈ 230 Hz for the cylinders. As further illustrated and similarly seen in previous studies on the SPCC [10–14], the SPCC exhibits similar spectral properties with a reduction of intensity of the dominant tonal peak and the clearer production of

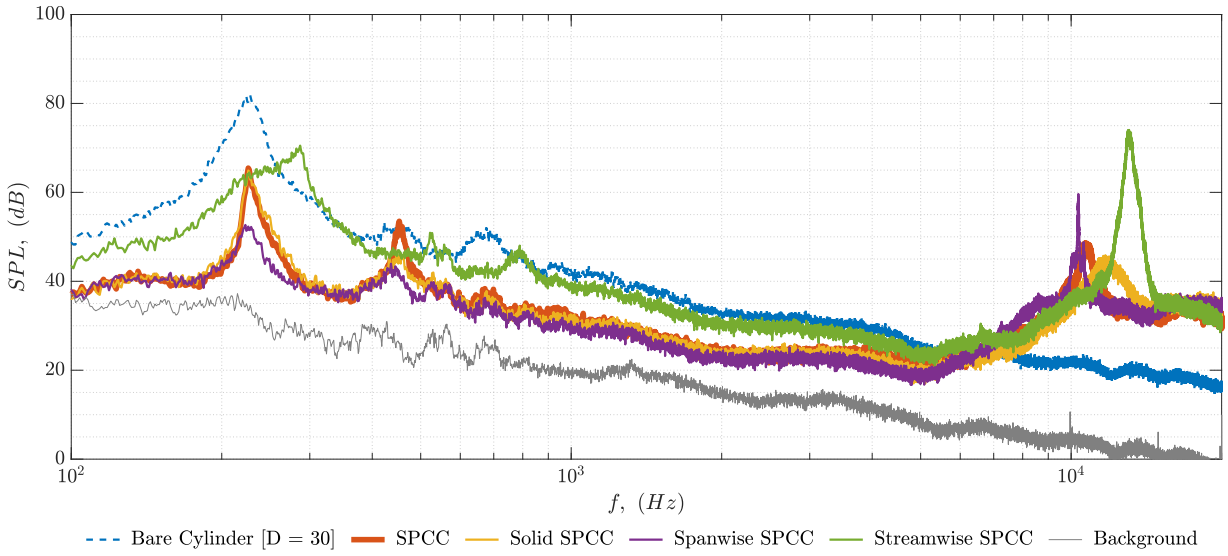

Fig. 11 SPCC, modified SPCCs and bare cylinder SPL recorded at $Re_D = 1 \times 10^5$.

a secondary tone, which will be referred to as the f_2 tone; at twice the vortex shedding frequency. This comparison also allows for a clearer presentation of the deviations in the spectral plots that the variations in geometry create. Comparing the purple and yellow plots, the original SPCC and Solid SPCC variations respectively, there is little variation in the acoustic results within the low to mid frequency ranges. Interestingly, the reduction of the spanwise communication has significantly improved the acoustic radiation from the cylinder with a reduction of $\approx$ 12 dB from the original SPCC and 30 dB over the baseline outer cylinder of the same outer diameter. The Streamwise SPCC spectra presented in green is an outlier due to the unique effects the variation has on the flow. With a matched diameter to the rest of the SPCC variants and bare cylinder the f_1 tone should be at the same frequency as the other spectra, this might be an effect of the stagnation regions within the SPCC's structure interfering with the natural vortex shedding behaviour.

C. Time-Averaged Wake Velocity Profiles

The first three figures within this section, Figs. 12,13 and 14 highlight the results gleaned from the time-averaged wake velocity profiles. Each figure presents the component profile of all comparable sized cylinders (D = 30 mm) measured within this experimental regime, the traverse grid of which is presented earlier in Fig. 5. Each streamwise location measured based on Figure 5 is presented in each figure, its specific location in the wake is highlighted in the caption corresponds to the letter subplots. Throughout this section, the blue line will represent the bare outer cylinder (D = 30 mm), the orange the original SPCC, the yellow the SPCC variation with the solid stagnation regions, the purple the SPCC variation in which the spanwise communication within the structure is blocked and lastly the Streamwise SPCC in green which blocks communication in the streamwise direction.

Starting with Fig. 12 which presents the normalised U component of the velocity within the wake region of the cylinders. Figs. 12(a) through (d) presenting similar characteristic velocity plots for x/D locations 0.75, 1, 1.5 and 2. Throughout this region of interest at a $y/D = \pm$ 1, each cylinder presented a region of increased velocity relative to the inflow velocity. It is clear from this figure that there are two groups within the cylinders tested, the bare cylinder and the similarly performing Streamwise SPCC, and the remaining three also present similar results to each other.

Through observation of the Fig. (a) thorough (g) focusing on the baseline bare Cylinder (blue) and Streamwise SPCC (green) it is clear that, as expected, the bare cylinder, has the smallest wake region which is consistent with prior works. Interestingly, to further prove the ability of the SPCC and the means by which it achieves noise reduction, the blockage of the streamwise communication within the SPCC's internal structure within the SPCC has reduced its performance to that of the bare cylinder. Prior works highlight the internal flow structure and vortex shedding off the inner cylinder, so the resulting velocity profiles of the bare cylinder and Streamwise SPCC throughout the observation region are to be expected.

Focusing on the second group of cylinders consisting of the Spanwise SPCC (purple), the Solid SPCC (yellow)

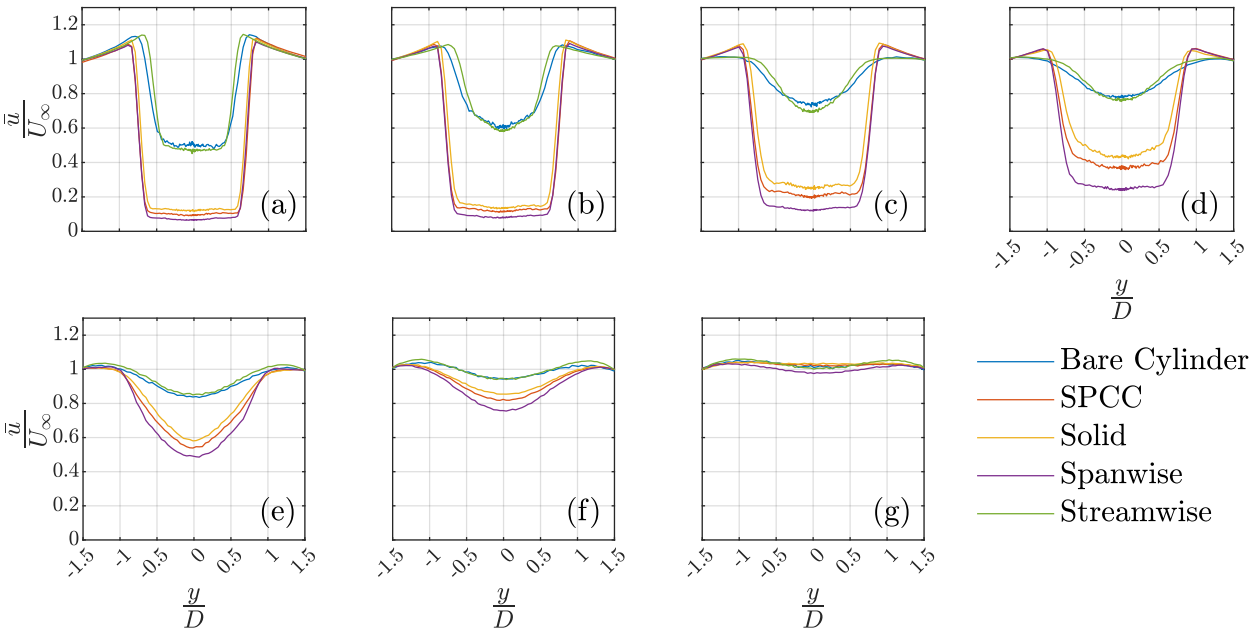

Fig. 12 Normalised time-averaged streamwise velocity, $\overline{u}/U_\infty$, at $Re_D = 1 \times 10^5$ and (a) x/D = 0.75, (b) x/D = 1, (c) x/D = 1.5, (d) x/D = 2, (e) x/D = 3, (f) x/D = 5 and (g) x/D = 7.

and the original SPCC (orange), it can be seen that throughout the Fig. (a) through (g) the cylinders perform with the same fundamental characteristics of the velocity profiles. However, the within the wake region, $-1 \leq y/D \leq 1$ the level of the reduced normalised velocity consistently deviates throughout all measured x/D locations; the Spanwise SPCC reduces the velocity within the stagnation region the most, followed by the original SPCC and finally followed by the Solid SPCC. This is most likely due to the friction drag the SPCC's impart on the flow based on each cylinder, the Solid SPCC likely reduces the drag due to the reduction in the stagnation regions and the inclusion of the aerodynamic shape within the SPCC structure thus increasing the velocity within the wake region. Alternatively the Spanwise SPCC blocks the internal communication between porous arrays by the inclusion of spanwise walls as highlighted in Fig. 3 could be increasing the drag imparted on the flow thorough the SPCC thus reducing the velocity within the stagnation region further but most likely increasing the overall drag of the SPCC.

Figure 13 and Fig. 14 present the normalised u_{rms} and v_{rms} velocity profiles which will help evaluate the magnitude of the fluctuations within the wake region of the developing flow downstream of the cylinders, and their corresponding intensities. Following a similar pattern to the previous section, the initial writings on Fig. 13 will focus on the the subplots (a) thorough (g) which correspond to the baseline bare cylinder (blue) and Streamwise SPCC (green) which present similar characteristics and peak locations with the highest presented turbulence intensities. From this exercise it is clear that, as similarly presented earlier in Fig. 12, the bare and Streamwise SPCC cylinders form the smallest wake regions with the highest turbulent intensities in both the U- and V-component throughout the initial experimental region. Most likely due to the smaller area in which the recirculating region develops, the later x/D locations present lower TI values than the optimal SPCC variants as the flow beings to settle downstream of the cylinders within the latter regions.

Following the trend of Fig. 12, the cylinders again form the two same groups, focusing on the optimal performing cylinders highlighted in purple, green and yellow, a similar trend can also be seen in this Fig. with the greatest reduction in the turbulence intensity (both U and V components) within the wake region being presented in the Spanwise SPCC variant, followed by the original SPCC followed by the Solid SPCC variant. This trend is present in both the TI_U and the TI_V measurements which present the wake region of the optimally modified SPCC's developing over a wider and longer region than the bare and Streamwise SPCC. Additionally, the region in which the vortex shedding behaviour first occurs is later within the wake, shown by the peaks of TI_v at low values of x/D, being of higher intensity than that of the modified SPCC's but also joining to make a singular large peak sooner within the experimental domain.

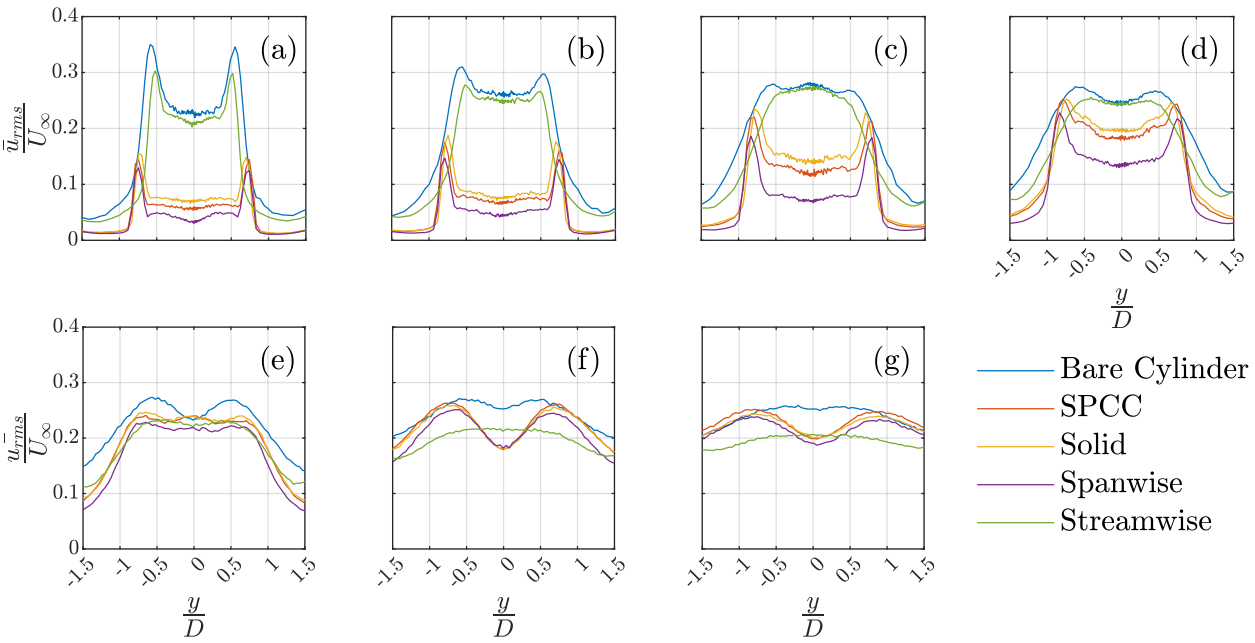

Fig. 13 Turbulence intensity of the streamwise velocity, $\overline{u}_{\text{rms}}/U_\infty$, recorded at $Re_D = 1 \times 10^5$ and (a) x/D = 0.75 (b) x/D = 1, (c) x/D = 1.5, (d) x/D = 2, (e) x/D = 3, (f) x/D = 5 and (g) x/D = 7.

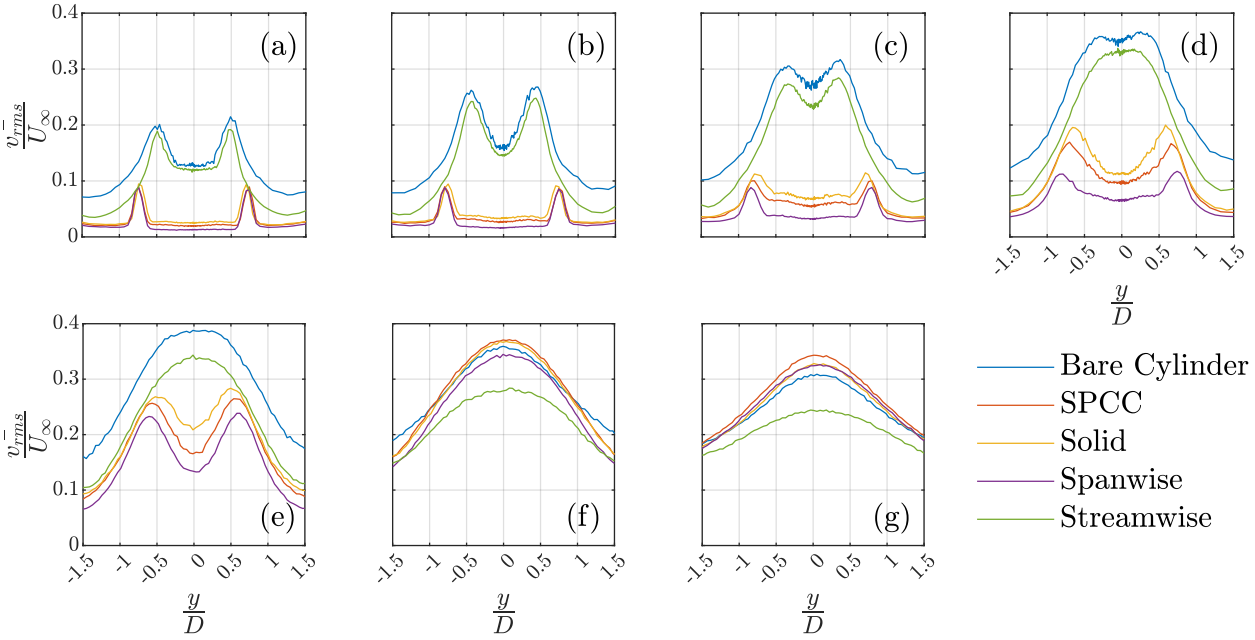

Fig. 14 Turbulence Intensity of the wall-normal velocity, $\overline{v}_{\text{rms}}/U_\infty$, recorded at $Re_D = 1 \times 10^5$ located at (a) x/D = 0.75 (b) x/D = 1, (c) x/D = 1.5, (d) x/D = 2, (e) x/D = 3, (f) x/D = 5 and (g) x/D = 7.

D. Wake velocity Power Spectral Density

Below in Figs. 15 and 16 the Welch's power spectral density estimate is presented for the significant tones, f_1 and f_2 and the spectral content at points A, B, C and D as specified by the square points within the Figures. In the first column of both figures, the colour represents the P_{uu} and P_{vv} values which are calculated following the equation: $10 * log_{10}(\sqrt{P_{xx}})$ for the f_1 tone, the central column the f_2 tone and the last column the spectral component of the velocity fluctuations at the points specified by A, B, C and D and corresponding to the colours in the legend. Additionally

in the last column is the dotted red line which highlights the f_2 tone and two dotted grey lines which represent the Strouhal number range first presented by Norberg [19]. Figs. 15(a - c), the first row corresponds to the baseline bare cylinder of the same outer dimension, D, and the latter SPCC variants. Row 2, 3, 4 and 5 correspond to the Streamwise , Original , Solid and Spanwise SPCC respectively. The positions of A, B, C and D are presented to more clearly compare the effects of the variants of the SPCC on the wake's formation. For the U component in Fig. 15 they are situated in the streamwise direction along the shear layer, in Fig. 16 they are positioned along the central line of the traverse grid where the V component will be strongest based on typical vortex shedding phenomena.

Focusing first of Figs. 15(a) and (d), presenting the f1 tone intensities throughout the traversal space for both the bare outer cylinder and Streamwise SPCC variant it can be seen that the intensity within the shear layer emanating from the bare cylinder is much larger and shows a similar trend as Figs. 13 and 14 and the characteristic shape and size of the wake are similar. Figure 15(f) also presents the peak frequencies at points A, B, C and D of the Streamwise SPCC to be outside of the expected Strouhal number range, unexpectedly the shedding frequency is larger than expected. Based off Equation 4, it was hypothesised that the stagnation regions created by the new modification would in essence enlarge the cylinders effective diameter, however, based on the equations, a higher frequency would occur with a smaller, D. Although an interesting results, due to the sub-optimal performance of the Streamwise SPCC, in addition to the unexpected vortex shedding performance it will no longer be considered within the remainder of the results analysis.

Figures 15(g), (j) and (m) allow the comparison between the original SPCC and optimal performing variants Solid and Spanwise SPCC respectively. As expected, by filling the estimated stagnation regions within the Solid SPCC the resultant P_{uu} is much higher, most likely due to the increased speed at which the shear layer emanates from the cylinder. Comparing Figs. 15(i) and (l) the spectral results between the SPCC and Solid SPCC are very similar other than a slight shift within the expected St number range and increase in the P_{uu} at the f_2 tone frequency which could account for the reduction in the acoustic SPL at the f_2 tone. In general the shapes of the wake region of Figs. 15(g), (j) and (m) are similar and aptly show the increased distance that the vortex shedding fluctuations occur layer within the measured domain. The best performing cylinder, presented in Figs. 15(m), (n) and (o), shows the peak P_{uu} at the f_1 and f_2 frequencies are over a wider range than that of the SPCC which presented not only more intense but also more narrow-band peaks in Fig. (i).

Figure 16 follows the same presentation style as Fig. 15 presenting the velocity power spectral density of the V-component within the wake region. Comparing row 1 (the baseline outer cylinder) to rows 3, 4 and 5 (the original SPCC, Solid SPCC and Spanwise SPCC) it is clear that the same characteristics shape of the wake region of the P_{vv} at both the f_1 and f_2 tone however the SPCC and its variants have delayed the development and elongated the wake. This can be seen clearly from point C in Figs. 16(i) and (o), comparing the original SPCC and the Spanwise SPCC that the peak intensity at the f_1 tone has been lowered by 6 dB. Looking at Figs. 16(g) and (h) allows us to compare the SPCC to the Solid region which was expected to make little change to the wake. As can be seen from the figure, although the intensity of the f_1 tone is larger, likely due to an increased speed as seen in earlier figures, the wake shape and characteristics are very similar including the spectral plots showing similar peaks and troughs in Figs. 16(i) and (l).

IV. Conclusion

In conclusion this paper presents the investigation into the effects of modifications to the internal structure of the SPCC would have on the vortex shedding tones and wake development relative to that of the original SPCC and bare cylinders of the same external diameter. It was found that, consistent with previous works, the geometric application of the structured porous geometry has been shown to provide ample reductions in respect to the bare cylinder counterparts. In addition, the three SPCC variants each presented unique aspects of the wake development and spectral characteristics. The three variants, the Streamwise SPCC (in which streamwise flow through the internal structure was blocked) further proved the importance of the internal flow within the structure of the SPCC and that the cylinders wake is dependant on the porous layer and the smaller internal diameters as the velocity components showed similar results of the Streamwise SPCC to the Baseline Outer Cylinder. The Solid SPCC was expected to change the results of the baseline SPCC minimally due to the filled regions only being that of the stagnation regions of the original SPCC. In accordance with the hypothesis, the Solid SPCC and original SPCC performed very similarly highlighting the importance of these stagnation regions and suggesting the possible mechanism by which the SPCC reduces vortex shedding tones. Lastly, to investigate the effects of the spanwise flow the Spanwise SPCC was designed to block the flow in the direction. Interestingly, at both f_1 and f_2 tones the cylinder vortex shedding noise had been reduced. This could be due to the additional walls within the SPCC's structure in the same direction of the flow could increase the spanwise coherence of the cylinder; this finding warrants further investigation and will be conducted in later works.

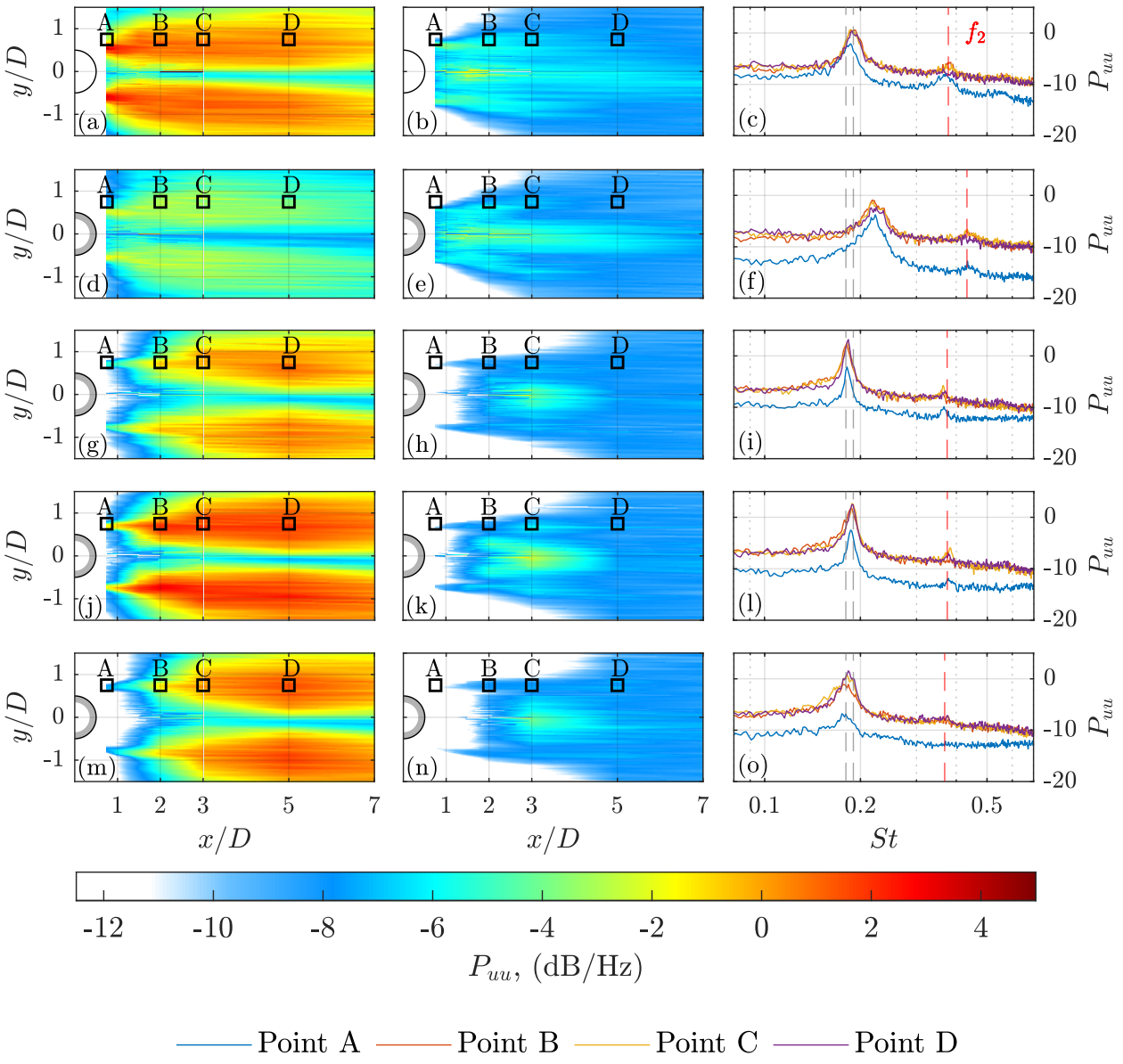

Fig. 15 PSD of streamwise velocity fluctuations recorded at $Re_D = 1 \times 10^5$. The left hand column corresponds to the PSD for the f_1 tone frequencies, P_{uu} (dB/Hz), the central column for the f_2 tone frequencies and the right column pertains to the spectral component of the velocity fluctuations at the points specified by A, B, C and D and corresponding to the colours in the legend. Points A, B, C and D are at the corresponding Coordinates x/D = 0.75, 2, 3 and 5 and a y/D values of 0.75 throughout. Rows 1, 2, 3, 4, and 5 correspond to the baseline outer cylinder followed by the Streamwise SPCC, Original SPCC, Solid SPCC and Spanwise SPCC respectively

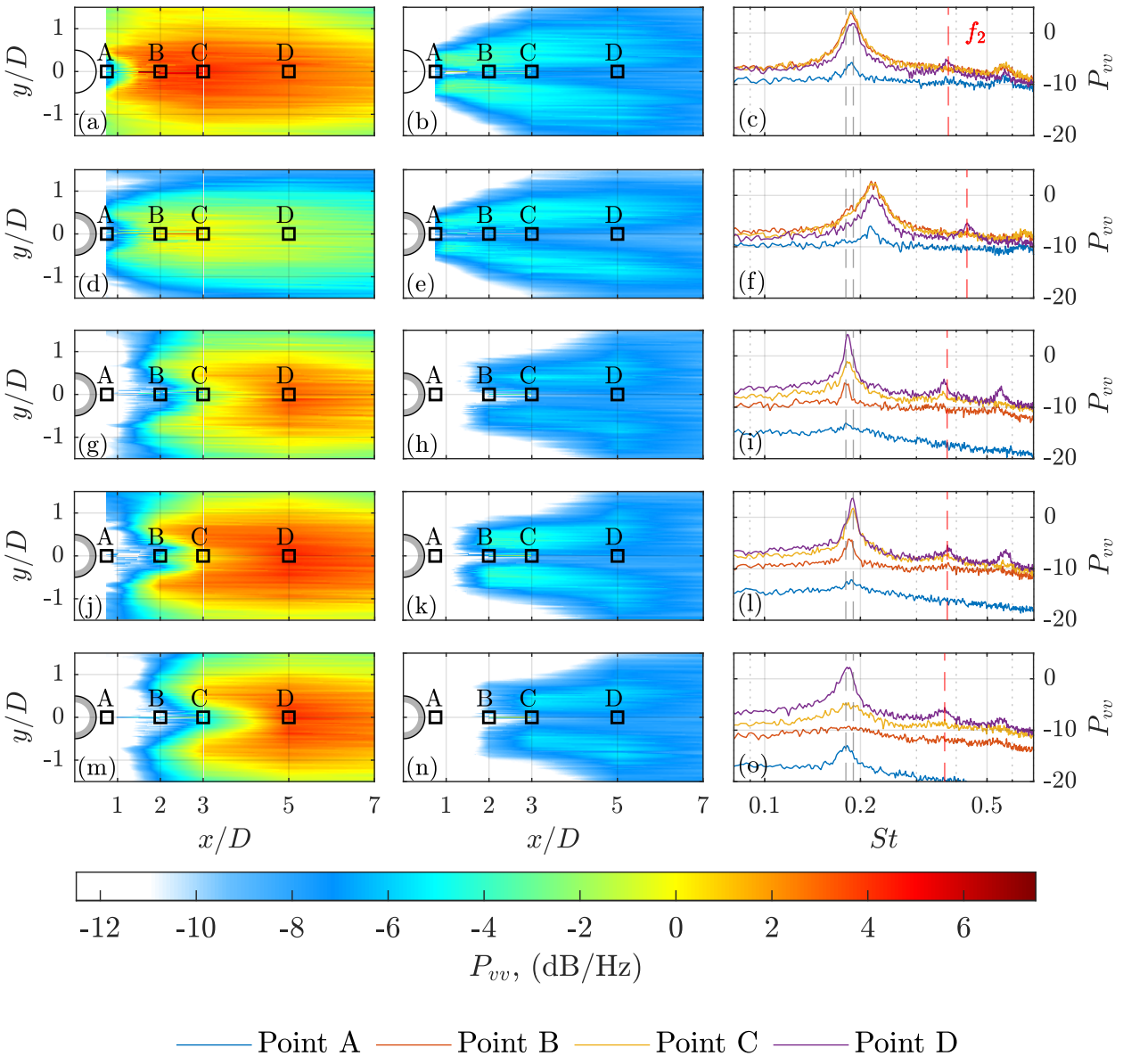

Fig. 16 PSD of wall-normal velocity fluctuations recorded at $Re_D = 1 \times 10^5$. The left hand column corresponds to the PSD for the f_1 tone frequencies, P_{vv} (dB/Hz), the central column for the f_2 tone frequencies and the right column pertains to the spectral component of the velocity fluctuations at the points specified by A, B, C and D and corresponding to the colours in the legend. Points A, B, C and D are at the corresponding Coordinates x/D = 0.75, 2, 3 and 5 and a y/D values of 0 throughout. Rows 1, 2, 3, 4, and 5 correspond to the baseline outer cylinder followed by the Streamwise SPCC, Original SPCC, Solid SPCC and Spanwise SPCC respectively

Acknowledgments

The authors would like to thank the EPSRC for the financial support from the Doctoral Training Partnership (DTP).

References

[1] SUEKI, T., IKEDA, M., and TAKAISHI, T., "Aerodynamic Noise Reduction using Porous Materials and their Application to High-speed Pantographs," *Quarterly Report of RTRI*, Vol. 50, No. 1, 2009, pp. 26–31. https://doi.org/10.2219/rtriqr.50.26.

[2] Boorsma, K., Zhang, X., Molin, N., and Chow, L. C., "Bluff Body Noise Control Using Perforated Fairings," *AIAA Journal*, Vol. 47, No. 1, 2009, pp. 33–43. https://doi.org/10.2514/1.32766.

[3] Etkin, B., Korbacher, G. K., and Keefe, R. T., "Acoustic Radiation from a Stationary Cylinder in a Fluid Stream (Aeolian Tones)," *The Journal of the Acoustical Society of America*, Vol. 29, No. 1, 1957, pp. 30–36. https://doi.org/10.1121/1.1908673.

[4] Casalino, D., and Jacob, M., "Prediction of aerodynamic sound from circular rods via spanwise statistical modelling," *Journal of Sound and Vibration*, Vol. 262, No. 4, 2003, pp. 815–844. https://doi.org/10.1016/s0022-460x(02)01136-7.

[5] Maryami, R., Ali, S. A. S., Azarpeyvand, M., and Afshari, A., "Turbulent flow interaction with a circular cylinder," *Physics of Fluids*, Vol. 32, No. 1, 2020, p. 015105. https://doi.org/10.1063/1.5119967.

[6] Wagner, H., Weger, M., Klaas, M., and Schröder, W., "Features of owl wings that promote silent flight," *Interface Focus*, Vol. 7, No. 1, 2017, p. 20160078. https://doi.org/10.1098/rsfs.2016.0078.

[7] Sagar, P., Teotia, P., Sahlot, A. D., and Thakur, H., "An analysis of silent flight of owl," *Materials Today: Proceedings*, Vol. 4, No. 8, 2017, pp. 8571–8575. https://doi.org/10.1016/j.matpr.2017.07.204.

[8] Sharma, S., Geyer, T. F., and Arcondoulis, E., "Effect of Coating Thickness on Aerodynamic Noise Reduction by Porous-Coated Cylinders," *28th AIAA/CEAS Aeroacoustics 2022 Conference*, American Institute of Aeronautics and Astronautics, 2022. https://doi.org/10.2514/6.2022-2889.

[9] Yuan, H., Xia, C., Chen, Y., and Yang, Z., "Flow around a Finite Circular Cylinder Coated with Porous Media," *54th AIAA Aerospace Sciences Meeting*, American Institute of Aeronautics and Astronautics, 2016. https://doi.org/10.2514/6.2016-0573.

[10] Arcondoulis, E. J. G., Liu, Y., Li, Z., Yang, Y., and Wang, Y., "Structured Porous Material Design for Passive Flow and Noise Control of Cylinders in Uniform Flow," *Materials*, Vol. 12, No. 18, 2019, p. 2905. https://doi.org/10.3390/ma12182905.

[11] Arcondoulis, E., Liu, Y., Geyer, T. F., Sedaghatizadeh, N., and Arjomandi, M., "Aeroacoustic performance of cylinders with a circumferential varying porous coating," *AIAA AVIATION 2020 FORUM*, American Institute of Aeronautics and Astronautics, 2020. https://doi.org/10.2514/6.2020-2527.

[12] Arcondoulis, E., Liu, Y., Li, Z., Yang, Y., Wang, Y., and Li, W., "The design and noise characteristics of a structured porous coated cylinder in uniform flow," *2018 AIAA/CEAS Aeroacoustics Conference*, American Institute of Aeronautics and Astronautics, 2018. https://doi.org/10.2514/6.2018-2963.

[13] Arcondoulis, E., Liu, Y., Yang, Y., Ragni, D., Carpio, A. R., and Avallone, F., "Internal and Near-Wall Flow Fields of a Structured Porous Coated Cylinder and Their Role in Passive Flow and Noise Control," *AIAA AVIATION 2021 FORUM*, American Institute of Aeronautics and Astronautics, 2021. https://doi.org/10.2514/6.2021-2226.

[14] Arcondoulis, E., Ragni, D., Carpio, A. R., Avallone, F., Liu, Y., Yang, Y., and Li, Z., "The internal and external flow fields of a structured porous coated cylinder and implications on flow-induced noise," *25th AIAA/CEAS Aeroacoustics Conference*, American Institute of Aeronautics and Astronautics, 2019. https://doi.org/10.2514/6.2019-2648.

[15] Xia, C., Wei, Z., Yuan, H., Li, Q., and Yang, Z., "POD analysis of the wake behind a circular cylinder coated with porous media," *Journal of Visualization*, Vol. 21, No. 6, 2018, pp. 965–985. https://doi.org/10.1007/s12650-018-0511-5.

[16] Naito, H., and Fukagata, K., "Numerical simulation of flow around a circular cylinder having porous surface," *Physics of Fluids*, Vol. 24, No. 11, 2012, p. 117102. https://doi.org/10.1063/1.4767534.

[17] Vathylakis, A., Chong, T. P., and Kim, J. H., "Design of a low-noise aeroacoustic wind tunnel facility at Brunel University," *20th AIAA/CEAS Aeroacoustics Conference*, American Institute of Aeronautics and Astronautics, 2014. https://doi.org/10.2514/6.2014-3288.

[18] Geyer, T., Sarradj, E., and Fritzsche, C., "Measurement of the noise generation at the trailing edge of porous airfoils," *Experiments in Fluids*, Vol. 48, No. 2, 2009, pp. 291–308. https://doi.org/10.1007/s00348-009-0739-x.

[19] Norberg, C., "Fluctuating lift on a circular cylinder: review and new measurements," *Journal of Fluids and Structures*, Vol. 17, No. 1, 2003, pp. 57–96. https://doi.org/10.1016/s0889-9746(02)00099-3.

[20] Arcondoulis, E., Liu, Y., Yang, Y., Ragni, D., Rubio Carpio, A., and Avallone, F., "Three dimensional internal and near-wall flow features of a structured porous coated cylinder," *28th AIAA/CEAS Aeroacoustics 2022 Conference*, 2022, p. 3038.